Analysis of electrical-field-dependent Dzyaloshinskii-Moriya interaction and magnetocrystalline anisotropy in a two-dimensional ferromagnetic monolayer

Jie Liu,[1,2,3,*] Mengchao Shi,[1,2] Jiwu Lu,[1,2,†] and M. P. Anantram[3]

[1]*College of Electrical and Information Engineering, Hunan University, Changsha 410082, People's Republic of China*

[2]*National Supercomputing Center in Changsha, Changsha 410082, People's Republic of China*

[3]*Department of Electrical Engineering, University of Washington, Seattle, Washington 98195, USA*

(Received 10 January 2018; published 16 February 2018)

We analyze the impacts of the electric field on the Dzyaloshinskii-Moriya interaction, magnetocrystalline anisotropy, and intrinsic ferromagnetism of the recently discovered two-dimensional ferromagnetic chromium tri-iodide (CrI_3) monolayer, by combining density functional theory and Monte Carlo simulations. By taking advantage of the counterbalancing effects of anisotropic symmetric exchange energy and antisymmetric exchange energy, it is shown that the intrinsic ferromagnetism can be manipulated by externally applied off-plane electric fields. The results quantitatively reveal the impacts of off-plane electric field on the lattice structure, magnetic anisotropy energy, symmetric and antisymmetric exchange energies, Curie temperature, magnetic hysteresis, and coercive field. The physical mechanism of all-electrical control of magnetism proposed here is useful for creating next-generation magnetic device technologies based on the recently discovered two-dimensional ferromagnetic crystals.

DOI: 10.1103/PhysRevB.97.054416

According to the Mermin-Wagner theorem, intrinsic magnetic order is not allowed at finite temperature in the $d \leqslant 2$-dimensional isotropic Heisenberg model. However, recent experimental observations and theoretical analysis have revealed that the magnetic anisotropy, which mainly originates from the spin-orbital coupling (SOC) effects, removes this restriction and permits intrinsic magnetic order at finite temperature in two-dimensional crystals like the chromium tri-iodide (CrI_3) monolayer [1–3]. Notably, these important discoveries have opened tremendous opportunities for creating novel magnetic sensor and data storage devices.

Technologically, it is vital to achieve size-compact and energy-efficient control of magnetism in semiconductor devices. Currently, externally applied magnetic fields and electric currents are the mainstream methods to manipulate magnetism in magnetic devices, e.g., hard disk and spin-transfer torque devices. However, these methods suffer from problems like high energy consumption and/or poor size compactness. By contrast, electrical-field/voltage control of magnetism has many advantages like low energy consumption and ultra-scalability [4]. Actually, the ability to control the materials' properties by external electric fields/voltages is at the heart of modern semiconductor device technologies [5]. Despite recent intensive research efforts, all-electrical control of magnetism in bulk and nanometer-scale materials is still a challenge that lies ahead [4–6]. In addition, how to electrically control magnetism in the recently discovered two-dimensional ferromagnetic crystals remains a brand-new open question [1,2].

In this paper, we propose an all-electrical physical mechanism to control the magnetism in the two-dimensional crystal CrI_3 monolayer, by applying an external electric field perpendicular to the monolayer. The control is achieved by the counterbalancing symmetric exchange effects and antisymmetric exchange effects, as can be seen in the *XXZ* Hamiltonian of the CrI_3 monolayer [3,7]:

$$H = \sum_{i \neq j} \left(\frac{1}{2} J \, \boldsymbol{S}_i \cdot \boldsymbol{S}_j + \frac{1}{2} \gamma \, S_{iz} S_{jz} + \frac{1}{2} \boldsymbol{D} \cdot (\boldsymbol{S}_i \times \boldsymbol{S}_j) \right) + \sum_i \mu_B \boldsymbol{B} \cdot \boldsymbol{S}_i . \quad (1)$$

Here, $\boldsymbol{S}_i$ is the spin of the ith Cr atom on the honeycomb Cr lattice and $|\boldsymbol{S}_i| = 3/2$; J is the Heisenberg isotropic symmetric exchange coefficient; γ is the anisotropic exchange coefficient; $\boldsymbol{D}$ is the Dzyaloshinskii-Moriya interaction (DMI) vector which represents the antisymmetric exchange effects [4,8–10]; μ_B is the Cr atom's magnetic moment; and $\boldsymbol{B}$ is the external magnetic field, which is set to zero everywhere in this paper except the hysteresis curve analysis.

To facilitate discussion, let us assume the CrI_3 monolayer is placed in the xy plane and the z axis is perpendicular to the monolayer. For the anisotropic exchange term in Eq. (1), the parallel/antiparallel alignment of spins along the z axis is the most energetically favorable configuration. This alignment can be ferromagnetic (parallel alignment) or antiferromagnetic (antiparallel alignment), up to the sign of γ, which mainly stems from the spin-orbital coupling effects in the ligand I atoms [3]. On the other hand, the antisymmetric exchange term energetically favors the spin-canting configuration, which attempts to arrange the spins perpendicular to each other [4,8–10]. The spin-canting effects tend to destroy the ferromagnetic (parallel alignment) or antiferromagnetic (antiparallel alignment) order established by symmetric exchange effects.

*liujie@uw.edu, jie_liu@hnu.edu.cn

†jiwu_lu@hnu.edu.cn

 ©2018 American Physical Society

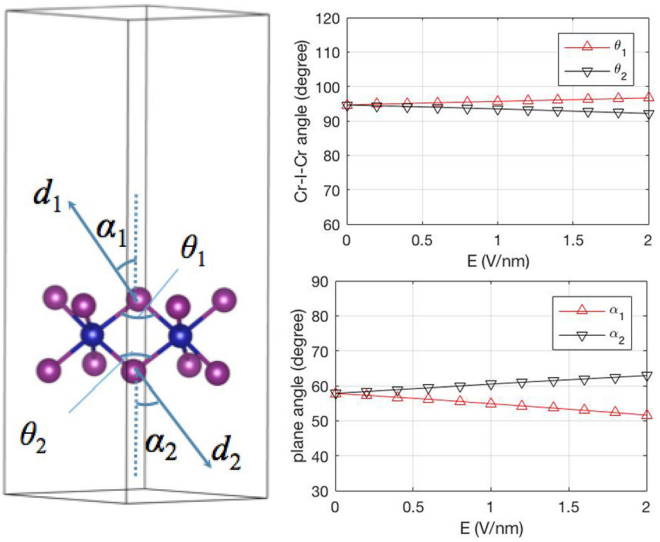


FIG. 1. Left: Unit cell of the CrI_3 monolayer. Right: Electric-field (E)-dependent Cr-I-Cr angles ($\boldsymbol{\theta}_1, \boldsymbol{\theta}_2$) and the tilting angles of Cr-I-Cr planes ($\boldsymbol{\alpha}_1, \boldsymbol{\alpha}_2$).

Without losing generality, here we assume that the external electric field $\boldsymbol{E}$ is pointing upward in the $+z$ direction. Driven by electrostatic effects, the positively charged Cr atoms move upward in the $+z$ direction, and the negatively charged I atoms move downward in the $-z$ direction. The breaking of inversion symmetry can be clearly seen in the $\boldsymbol{E}$ dependence of the Cr-I-Cr angles (θ_1, θ_2) and the tilting angles of the Cr-I-Cr planes (α_1, α_2). For each pair of Cr atoms, as shown in Fig. 1, the upper and lower bonded I atoms form local DMI vectors $\boldsymbol{d}_1$ and $\boldsymbol{d}_2$, respectively. When the external electric field $\boldsymbol{E} = 0$, $\boldsymbol{d}_1$ and $\boldsymbol{d}_2$ cancel each other due to symmetry, leading to vanishing gross antisymmetric exchange effects, i.e., $\boldsymbol{D} = 0$. When an electric field $\boldsymbol{E} \neq 0$ is applied perpendicular to the monolayer, $\boldsymbol{D} \neq 0$ due to the breaking of inversion symmetry [3].

Here, the $\boldsymbol{E}$-dependent lattice structures are obtained by spin-polarized density functional theory (DFT) calculations using QUANTUM ESPRESSO [11]. The projector augmented wave pseudopotential [12] and the Perdew-Burke-Ernzerhof exchange-correlation functional [13] are applied; the kinetic-energy cutoff values for wave functions and charge density are chosen as 48.0 and 457.0 Ry, respectively. The supercell size in the z direction is set as 4.0 nm, leaving enough vacuum space to separate the CrI_3 monolayers due to the artificial periodic boundary condition in the z direction. To include an off-plane electric field, a sawlike potential and a dipole correction are added to the bare ionic potential along the z direction [14]. The atomic lattice relaxation continues until all residue atomic forces are smaller than 10^{-4} hartree/bohr (about 5 meV/Å). The electronic self-consistency convergence criterion is set as 10^{-12} Ry, in order to accurately capture the energetically subtle magnetic effects.

From the $\boldsymbol{E}$-dependent DFT calculations, the magnetic moments of Cr atoms (μ_B) and the total energies can be obtained. As shown in Fig. 2, μ_B is only slightly decreased when $|\boldsymbol{E}|$ is increased, and the ferromagnetic state is more energetically favorable than the antiferromagnetic state. These indicate robust ferromagnetism in the two-dimensional CrI_3 monolayer under external off-plane electric fields.

To evaluate the $\boldsymbol{E}$-dependent magnetic anisotropy energy (MAE), the force theorem implemented in QUANTUM ESPRESSO is used [15]. First, the two spins of the two Cr atoms in the unit cell are fixed in the off-plane direction. Second, the two spins are fixed in the in-plane direction. It is found that the off-plane direction (i.e., easy axis) is more energetically favorable than the in-plane direction, and the calculated $\boldsymbol{E}$-dependent MAE is shown in Fig. 3. To evaluate the $\boldsymbol{E}$-dependent isotropic/anisotropic symmetric exchange coefficient J/γ, spins are aligned parallel or antiparallel to each other such that the antisymmetric exchange term in Eq. (1) vanishes. Using MAE values and the comparative energy difference between the ferromagnetic state and antiferromagnetic state (Fig. 2), J and γ can be calculated as shown in Fig. 3.

Qualitatively, the $\boldsymbol{E}$-induced breaking of inversion symmetry makes $|\boldsymbol{d}_1| \neq |\boldsymbol{d}_2|$, leading to a nonzero DMI vector $|\boldsymbol{D}| \neq 0$, as shown in Fig. 1 and Eq. (1) [3]. Due to the nonzero tilting angle of the Cr-I-Cr plane, the DMI vector $\boldsymbol{D}$ has an in-plane component D_{xy} and an off-plane component D_z, as shown in Fig. 4. Interestingly, each Cr atom is bonded to six adjacent I atoms, so the in-plane components D_{xy} rotate around the Cr atoms. The rotating direction is clockwise around one Cr atom in the unit cell and counterclockwise around the other Cr atom.

Quantitatively, the two Cr-I-Cr planes associated with a pair of Cr atoms have the same tilting angles ($\alpha_1 = \alpha_2$) when

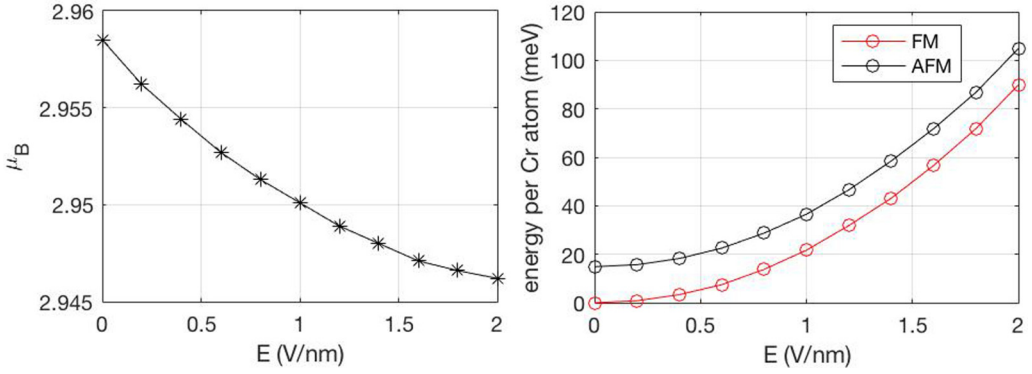


FIG. 2. Left: Magnetic moment or the Cr atom in the Bohr magneton. Right: Comparative total energies of the ferromagnetic (FM) state and antiferromagnetic (AFM) state.

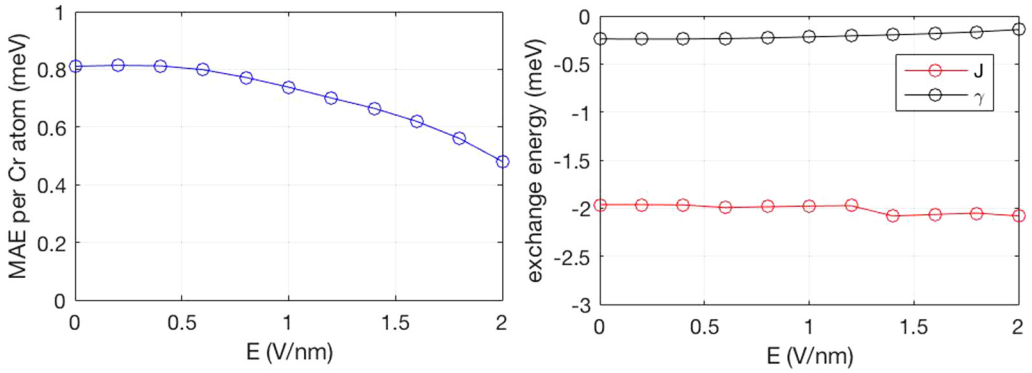


FIG. 3. Left: Magnetic anisotropy energy (MAE). Right: Heisenberg isotropic symmetric exchange coefficient J and anisotropic symmetric exchange coefficient $\boldsymbol{\gamma}$.

$\boldsymbol{E} = 0$. When $\boldsymbol{E} \neq 0$, however, $\alpha_1 \neq \alpha_2$ but the difference is very small. For example, $\alpha_1 - \alpha_2 \approx 5.6^\circ$ when $|\boldsymbol{E}| = 1.0\,\mathrm{V/nm}$. Thus, we can use the relations $\alpha = (\alpha_1 + \alpha_2)/2$ and $D_{xy}/D_z = \tan(\alpha)$ to approximately evaluate the strength of $\boldsymbol{D}$. To evaluate D_z, the spins of the two Cr atoms in the unit cell are constrained in the xy plane, as shown in Fig. 4. One spin is aligned along the x axis, and the other has an angle $\Delta\theta \neq 0$ with respect to the x axis. The total energy can be written as

$$E(\Delta\theta) = E_0 + J\,\tfrac{1}{2}\,n\,|S|^2\cos(\Delta\theta) + D_z\,\tfrac{1}{2}\,n\,|S|^2\sin(\Delta\theta) \quad (2)$$

using Eq. (1). Here, $E(\Delta\theta)$ is computed using the fully relativistic self-consistent-field DFT calculations including both SOC and noncollinear spin-polarization effects; E_0 is a constant; $|\boldsymbol{S}| = 3/2$; and $n = 6$ is the number of Cr-Cr edges associated with the two Cr atoms in the unit cell in the Cr honeycomb lattice. Therefore, using two self-consistent-field DFT calculations' total energies, $E(\Delta\theta)$ and $E(-\Delta\theta)$, the first two terms can be eliminated and D_z can be evaluated. Theoretically, under a particular $\boldsymbol{E}$, D_z should be a constant and independent of $\Delta\theta$. This is numerically verified as shown in the $D_z(\Delta\theta)$ plot of Fig. 4. It is also verified that this independence is valid for different $\boldsymbol{E}$ values. Then, D_{xy} can be evaluated using $D_{xy} \approx D_z \tan[(\alpha_1 + \alpha_2)/2]$.

The externally applied off-plane electric field has two effects. First, $|\boldsymbol{D}|$ is increased when $|\boldsymbol{E}|$ is increased as shown in Fig. 4, indicating that the electric field enhances the spin-canting effects. Second, as shown in Fig. 3, the electric field attenuates MAE and anisotropic symmetric exchange effects. Both effects attenuate the ferromagnetic ordering, which can be utilized to control magnetism.

To quantitatively investigate the strength of control, the Metropolis Monte Carlo (MMC) method is used to compute the ground state of Eq. (1) [16]. As shown in Fig. 5, the net magnetization is reduced as temperature increases. When $|\boldsymbol{E}| = 0$, the simulated Curie temperature $T_C \approx 40\,\mathrm{K}$. As a comparison, the measured $T_C \approx 45\,\mathrm{K}$ [1]. When $|\boldsymbol{E}|$ is increased, the magnetization is slightly attenuated, indicating weakened ferromagnetic order. However, the T_C is not decreased significantly, indicating that the off-plane electric field has limited impacts on the temperature dependence of magnetization.

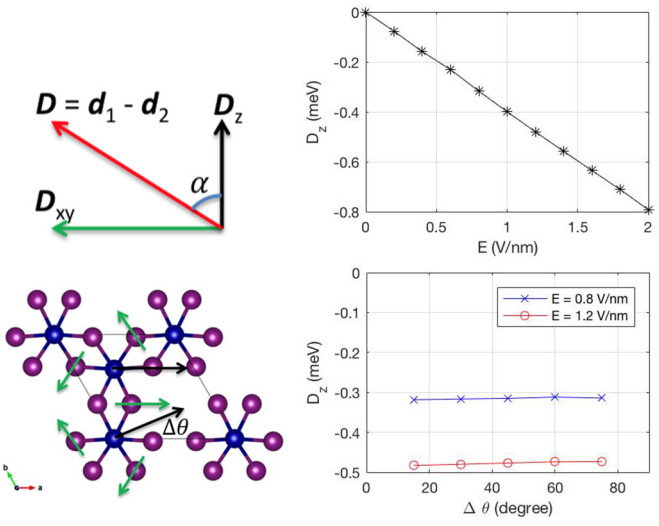


FIG. 4. Illustrative figures for computing the in-plane component (D_{xy}) and off-plane component (D_z) of the DMI vector.

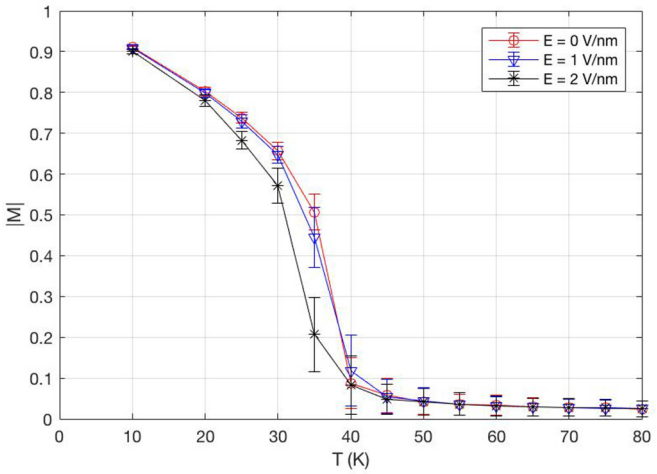


FIG. 5. Temperature-dependent magnetization curves under different perpendicular electric field E, simulated using the Metropolis Monte Carlo method. The marked point and error bar stand for the mean and standard deviation of 1000 simulated samples, respectively. The initial spins are random three-dimensional vectors.

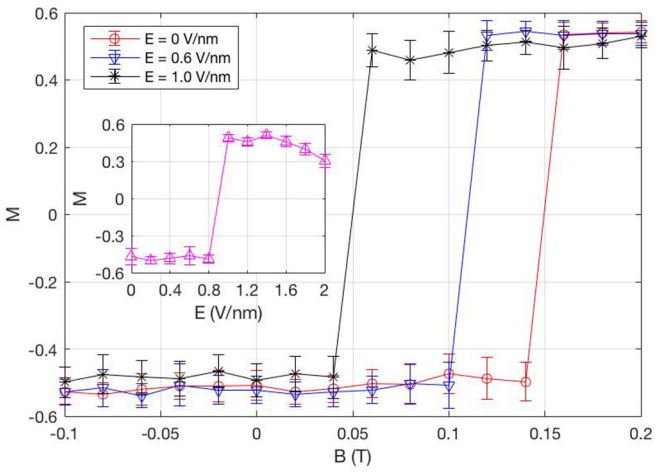


FIG. 6. Hysteresis curves under different perpendicular electric field E, simulated using the Metropolis Monte Carlo method. The marked point and error bar stand for the mean and standard deviation of 1000 simulated samples, respectively. The initial spins all point to the $-z$ direction. Inset: The magnetization M initially pointing in the $-z$ direction can be flipped by increasing the electric field E (simulated under $T = 35\,\mathrm{K}$ and $B = 0.06\,\mathrm{T}$).

By contrast, using MMC simulations [17] it can be seen that the off-plane electric field has much more significant impacts on the hysteresis curve and coercive field B_c. When $|\boldsymbol{E}| = 0$, the simulated $B_c = 0.14{-}0.16\,\mathrm{T}$. Note that the reported measured B_c varies between 0.05 and 0.2 T [1]. The variation might be caused by strain or charge puddles formed when the CrI_3 monolayer is exfoliated onto the SiO_2/Si substrate [1]. When $|\boldsymbol{E}|$ is increased, B_c drops obviously as shown in Fig. 6. This means that, with the assistance of an off-plane electric field, the ferromagnetism is weakened and the ferromagnetic configuration can be flipped much more easily. The electrical control of magnetism can be seen more directly in the inset of Fig. 6. By increasing the off-plane electric field, the $-z$ direction initial magnetization of the CrI_3 monolayer can be flipped into $+z$ direction.

From the above analysis, it can be seen that the electrical control strength of magnetism could be influenced by multiple factors, which deserve future research attention to optimize material and device performance. It is known that, though the magnetization comes directly from the spins on the honeycomb Cr lattice, both the antisymmetric exchange effects and the anisotropic symmetric exchange effects actually originate from the SOC effects of the ligand I atoms [3]. So it may strengthen/weaken control strength by choosing heavier/lighter ligand atoms, which have stronger/weaker SOC effects. The $\boldsymbol{E}$-induced breaking of inversion symmetry is the fundamental reason for the electrical control of magnetism. So the control strength may be tuned by choosing materials with different electric polarity and bond strength, as they influence the magnitude of $\boldsymbol{E}$-induced lattice distortion.

We acknowledge Dr. Xiaodong Xu for useful discussion [1]. Jie Liu gratefully acknowledges the Fundamental Research Funds for the Central Universities of People's Republic of China for supporting this research. The calculations were performed using the supercomputers in the National Supercomputing Center in Changsha, People's Republic of China. We would like to thank Dr. Xianzhong Duan, Dr. Min He, Dr. Kenli Li, and Dr. Can Leng for their help.

[1] B. Huang, G. Clark, E. Navarro-Moratalla, D. R. Klein, R. Cheng, K. L. Seyler, D. Zhong, E. Schmidgall, M. A. McGuire, D. H. Cobden, W. Yao, D. Xiao, P. Jarillo-Herrero, and X. Xu, Layer-dependent ferromagnetism in a van der Waals crystal down to the monolayer limit, Nature (London) **546**, 270 (2017).

[2] C. Gong, L. Li, Z. Li, H. Ji, A. Stern, Y. Xia, T. Cao, W. Bao, C. Wang, Y. Wang, Z. Q. Qiu, R. J. Cava, S. G. Louie, J. Xia, and X. Zhang, Discovery of intrinsic ferromagnetism in two-dimensional van der Waals crystals, Nature (London) **546**, 265 (2017).

[3] J. L. Lado and J. Fernández-Rossier, On the origin of magnetic anisotropy in two dimensional CrI_3, 2D Mater. **4**, 035002 (2017).

[4] A. Fert, N. Reyren, and V. Cros, Magnetic skyrmions: Advances in physics and potential applications, Nat. Rev. Mater. **2**, 17031 (2017).

[5] K. S. Novoselov, Electric field effect in atomically thin carbon films, Science **306**, 666 (2004).

[6] F. Matsukura, Y. Tokura, and H. Ohno, Control of magnetism by electric fields, Nat. Nanotechnol. **10**, 209 (2015).

[7] W.-B. Zhang, Q. Qu, P. Zhu, and C.-H. Lam, Robust intrinsic ferromagnetism and half semiconductivity in stable two-dimensional single-layer chromium trihalides, J. Mater. Chem. C **3**, 12457 (2015).

[8] I. Dzyaloshinsky, A thermodynamic theory of weak ferromagnetism of antiferromagnetics, J. Phys. Chem. Solids **4**, 241 (1958).

[9] T. Moriya, Anisotropic superexchange interaction and weak ferromagnetism, Phys. Rev. **120**, 91 (1960).

[10] S.-W. Cheong and M. Mostovoy, Multiferroics: A magnetic twist for ferroelectricity, Nat. Mater. **6**, 13 (2007).

[11] P. Giannozzi, S. Baroni, N. Bonini, M. Calandra, R. Car, C. Cavazzoni, D. Ceresoli, G. L. Chiarotti, M. Cococcioni, I. Dabo, A. D. Corso, S. de Gironcoli, S. Fabris, G. Fratesi, R. Gebauer, U. Gerstmann, C. Gougoussis, A. Kokalj, M. Lazzeri, L. Martin-Samos, N. Marzari, F. Mauri, R. Mazzarello, S. Paolini, A. Pasquarello, L. Paulatto, C. Sbraccia, S. Scandolo, G. Sclauzero, A. P. Seitsonen, A. Smogunov, P. Umari, and R. M. Wentzcovitch, QUANTUM ESPRESSO: A modular and open-source software project for quantum simulations of materials, J. Phys.: Condens. Matter **21**, 395502 (2009).

[12] P. E. Blochl, Projector augmented-wave method, Phys. Rev. B **50**, 17953 (1994).

[13] J. P. Perdew, K. Burke, and M. Ernzerhof, Generalized Gradient Approximation Made Simple, Phys. Rev. Lett. **77**, 3865 (1996).

[14] L. Bengtsson, Dipole correction for surface supercell calculations, Phys. Rev. B **59**, 12301 (1999).

[15] D. Li, C. Barreteau, M. R. Castell, F. Silly, and A. Smogunov, Out- versus in-plane magnetic anisotropy of free Fe and Co nanocrystals: Tight-binding and first-principles studies, Phys. Rev. B **90**, 205409 (2014).

[16] N. Metropolis, A. W. Rosenbluth, M. N. Rosenbluth, A. H. Teller, and E. Teller, Equation of state calculations by fast computing machines, J. Chem. Phys. **21**, 1087 (1953).

[17] R. F. L. Evans, W. J. Fan, P. Chureemart, T. A. Ostler, M. O. A. Ellis, and R. W. Chantrell, Atomistic spin model simulations of magnetic nanomaterials, J. Phys.: Condens. Matter **26**, 103202 (2014).